# 7A52 铝合金水蒸气等离子弧焊接头组织及性能

马世宁， 罗 林， 邱 骥， 刘 谦
（装甲兵工程学院 装备再制造工程系，北京 100072）

马世宁

摘 要：采用水蒸气等离子电弧技术对 10 mm 厚的 7A52 铝合金板材进行焊接试验，焊接介质为 40% 丙酮水溶液，焊丝为 ER5356，对焊接接头的力学性能进行了测试分析，对焊接接头的显微组织进行了分析．结果表明，7A52 铝合金水蒸气等离子弧焊接头性能较好，焊缝拉伸断口表面存在大量的韧窝，表明焊缝有良好的韧性；热影响区存在软化区域；焊接接头熔合良好，焊缝没有发现异常的气孔、夹渣和裂纹等焊接缺陷．利用水蒸气等离子弧技术焊接 7A52 铝合金可以得到优良的焊接接头．

关键词：7A52 铝合金；水蒸气等离子弧焊；焊接接头；显微组织
中图分类号：TG406 TG456.2 文献标识码：A 文章编号：0253－360X(2009)09－0009－04

## 0 序 言

7A52 铝合金是近年来国内自行研制的装备结构材料，是一种具有中等强度可热处理强化的可焊铝合金．该合金经轧制能获得比较理想的板材，通过适当固溶和回归再时效处理，可获得优良的综合性能，已批量应用于军用装备、航空航天器与地面车辆等焊接构件[1－3]．目前 7A52 铝合金结构焊接主要采用熔化极氩弧焊和搅拌摩擦焊工艺．熔化极氩弧焊热输入大，主要用于 7A52 铝合金焊接结构的生产．搅拌摩擦焊是一种固相焊接技术，可降低或避免熔焊时产生的焊接缺陷，该技术对工装设备及焊缝形状要求较高．但是以上两种工艺均不适合于铝合金结构在野外条件下的应急维修焊接作业．

水蒸气等离子弧技术是利用水或其它介质水溶液通过加热蒸发，产生气体介质，在强电场作用下产生电弧，由于喷嘴的机械压缩作用、气流的冷却和压缩作用以及自身的磁收缩作用等，使电弧得到压缩，形成具有等离子弧特征的电弧[4,5]．它具有节能、环保、便携、高效等特点，焊接时不需要惰性气体保护，工艺简单，特别适合于野外应急维修焊接．但是，国内外关于水蒸气等离子弧焊接铝合金方面的报道较少，没有关于这种技术针对铝合金焊接工艺方面的研究可以借鉴．为此，采用水蒸气等离子弧焊接工艺对 7A52 铝合金进行焊接，对其焊接接头性能进行了测试分析，并对其微观组织结构进行了分析和研究．

收稿日期：2008－07－04
基金项目：装备再制造技术国防科技重点实验室基金项目（9140C8504020808）

## 1 试验方法

试验选用 10 mm 厚的 7A52 铝合金板材，状态为淬火人工时效状态（CS），抗拉强度 $R_m \geqslant 410$ MPa，断后伸长率 $A \geqslant 7\%$．采用 $\phi$3 mm ER5356 焊丝进行焊接，基体及焊丝的主要化学成分见表 1 和表 2．

表 1 7A52 铝合金主要化学成分（质量分数，%）
Table 1 Chemical composition of 7A52 aluminum alloy

| Si | Cu | Mn | Mg | Zn |
|---|---|---|---|---|
| 0.25 | 0.05～0.20 | 0.20～0.50 | 2.0～2.8 | 4.0～4.8 |
| Fe | Cr | Ti | Zr | Al |
| 0.30 | 0.15～0.25 | 0.05～0.18 | 0.05～0.15 | 余量 |

表 2 ER5356 焊丝主要化学成分（质量分数，%）
Table 2 Chemical composition of ER5356 filler

| Si | Cu | Mn | Mg | Zn |
|---|---|---|---|---|
| 0.25 | 0.10 | 0.20～0.50 | 4.5～5.5 | 0.10 |
| Fe | Cr | Ti | 其它 | Al |
| 0.40 | 0.15～0.25 | 0.05～0.15 | 0.05～0.15 | 余量 |

试验采用水蒸气等离子弧焊接设备，其设备工作原理见图 1．采用 80°V 形坡口进行对接焊，焊前对坡口表面进行打磨处理，然后用乙醇进行清洗，自

然晾干后将焊剂涂覆在对接坡口表面，单面一次焊完，焊接工艺见表 3. 焊接介质为 40%丙酮水溶液.

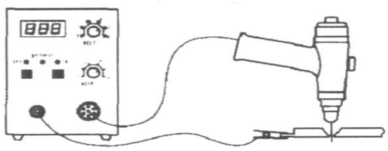

图 1 水蒸气等离子弧设备示意图

Fig. 1 Schematic of vapor plasma arc welding equipment

表 3 水蒸气等离子弧焊接工艺参数

Table 3 Welding parameters of vapor plasma arc welding

| 电弧电压 $U$/V | 焊接电流 $I$/A | 焊接速度 $v$/(cm·min$^{-1}$) | 喷嘴距焊缝距离 $d$/mm |
|---|---|---|---|
| 220±10% | 直流 3.4~12 | 50~70 | 2~4 |

拉伸试样沿焊缝横向取样，在 CSS —2210 —1 电子万能试验机上进行试验；采用 HVS —1000 型数显显微硬度计进行接头显微硬度检测；分别采用 OLYMPUS — BX41 型光学金相显微镜及 Quanta2000 型扫描电镜观察接头显微组织和断口形貌；接头微区成分分析采用 GENESIS 型能谱仪进行分析. 制样所用腐蚀液为 5 mL $HNO_3$+3 mL HF+92 mL $H_2O$ 溶液.

## 2 试验结果及讨论

### 2.1 接头抗拉强度

焊接接头的抗拉强度见表 4，最高为 303 MPa，达基体强度的 74%，平均为 250 MPa，达基体强度的 61%. 接头拉伸试验断裂位置均出现在焊缝处.

表 4 7A52 铝合金焊接接头抗拉强度

Table 4 Tensile strength of vapor plasma arc welding joints

| 试样 1 $R_{m1}$/MPa | 试样 2 $R_{m2}$/MPa | 试样 3 $R_{m3}$/MPa | 试样 4 $R_{m4}$/MPa | 平均值 $R_m$/MPa |
|---|---|---|---|---|
| 303 | 230 | 223.2 | 245 | 250.3 |

水蒸气等离子弧具有高温特性，焊接时弧柱中心温度达 8 000 K 以上，使焊丝与局部基材充分熔化，同时由于水蒸气等离子弧弧柱挺度好，焊接过程中电弧吹力对熔池具有强烈的搅拌作用，使得熔融的液态金属充分对流、混合，这对减少焊缝气孔和提高接头强度十分有利.

### 2.2 显微硬度

接头显微硬度测试由焊缝(宽度约为 11 mm)中心向基体一侧进行，显微硬度(HV1.96)分布如图 2 所示. 由图 2 可见，7A52 铝合金基体显微硬度为 120 HV1.96，焊缝显微硬度最低，约为 92 HV1.96；热影响区宽度约为 20 mm，其靠近焊缝侧的显微硬度略高于基体，而软化区域的显微硬度略低于基体.

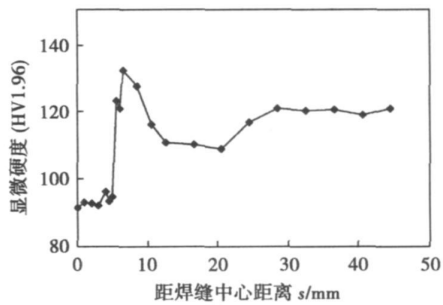


图 2 焊接接头显微硬度(HV1.96)分布

Fig. 2 Surface hardness distribution of welded joint

试验结果表明，利用水蒸气等离子弧焊接时，在靠近焊缝的小区内，由于峰值温度高以及焊后快速冷却，导致该区发生固溶(淬火)，导致显微硬度升高. 而距离焊缝较远的区域由于焊接时峰值温度相对较低以及冷却速度相对较慢，致使该处晶粒粗化，显微硬度降低，出现软化区域.

### 2.3 接头拉伸断口分析

焊接接头的典型拉伸断口形貌如图 3 所示. 断口上没有明显的放射区，而是呈现出大面积很深的等轴形韧窝，大韧窝中包含着许多小韧窝，大韧窝的直径约是小韧窝的 3~4 倍；在剪切唇区可见到明显的延性棱(图 3 中白色箭头所示)，说明材料在局部微小区域内发生了强烈的塑性变形[9]. 表明由水蒸气等离子弧焊接的 7A52 铝合金焊缝塑性较好，其断裂形式为韧性断裂.

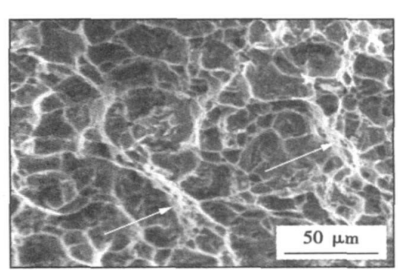


图 3 7A52 拉伸断口 SEM 形貌

Fig. 3 SEM micrograph of tensile fracture of welded joint

### 2.4　显微组织及能谱分析

7A52 铝合金水蒸气等离子弧焊接头由基体、热影响区、熔合区和焊缝区组成. 图 4 是各区光学金相显微组织形貌.

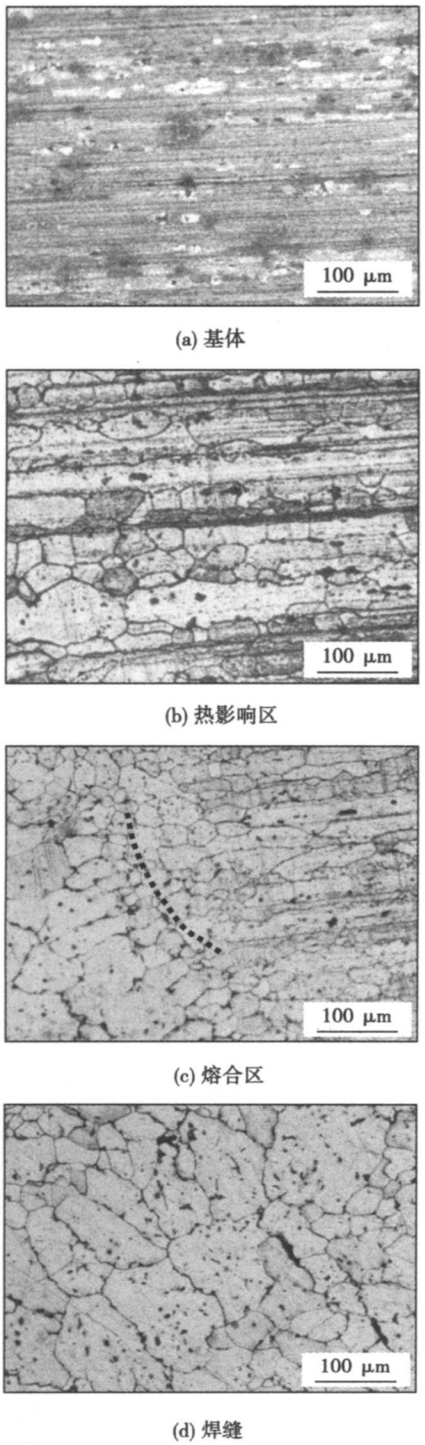


图 4　7A52 铝合金焊接接头显微组织

Fig. 4　Microstructures of 7A52 aluminum alloy welded joint

图 4a 为 7A52 铝合金基体，呈现板条带状 α＋T 相组织，其主要强化机制是析出强化，合金强度主要由强化相的大小、数量和弥散度决定[7,8]；热影响区(图 4b)在焊接热输入的影响下出现不同程度的组织粗化现象，但条带状组织仍清晰可见，只是板条明显变厚，其组织为 α(Al)固溶体，黑色质点为析出的 T($Al_2Zn_3Mg_3$)相[9]；从图 4c 可以看出，接头存在明显的熔合区，图中右侧靠近热影响区，左侧靠近焊缝，可见粗骨骼状 β($Mg_5Al_8$)相柱状晶带垂直于熔合线(图中黑色虚线)向焊缝内部生长，熔合区熔合良好，没有异常的气孔、夹渣、裂纹等缺陷；焊缝(图 4d)中等轴晶、条状晶及块状晶共存，这些晶粒大小不一，为 α(Al)固溶体，图中黑色点状析出物质为 T($Al_2Zn_3Mg_3$)相和 η($MgZn_2$)，焊缝中也没有发现明显异常的气孔、夹渣、焊接热裂纹等缺陷.

焊缝微区能谱检测位置见图 5 中方框所示，其元素成分如表 5 所示. 从表中可以看出，熔合区附近锌和镁的含量均介于热影响区和焊缝之间，其中锌的含量从热影响区到焊缝是逐渐减少的，而镁的含量则逐渐增加，说明在焊缝熔池形成过程中，熔融的焊丝与熔化的基材在水蒸气等离子电弧吹力、液态金属密度差以及表面张力等因素的作用下，两者进行了强烈对流运动和混合[10]，在靠近基体的微区中(熔合区附近)锌、镁等元素进行了充分相互扩散，焊接接头熔合良好，7A52 铝合金水蒸气等离子弧焊属冶金结合.

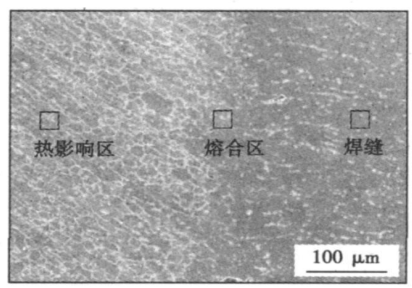


图 5　焊接接头能谱检测位置

Fig. 5　Chemical compositions of the welded joint from EDAX

表 5　图 5 中不同微区能谱分析(质量分数，%)

Table 5　EDAX compositions of different zones in Fig. 5

| | Zn | Mg |
|---|---|---|
| 热影响区 | 4.64 | 3.12 |
| 熔合区 | 3.33 | 3.84 |
| 焊缝 | 1.45 | 5.52 |

## 3　结　　论

(1) 采用水蒸气等离子弧焊接工艺，7A52 铝合

金焊接接头抗拉强度可达 303 MPa，为 7A52 铝合金强度的 74%.

(2) 7A52 铝合金水蒸气等离子弧焊接头熔合良好，焊缝具有良好的韧性，焊缝中没有明显的气孔、夹渣、裂纹等焊接缺陷.

(3) 热影响区中靠近焊缝的微区由于焊接时峰值温度高及随后的快速冷却导致该区发生固溶，显微硬度升高；而距焊缝较远处由于晶粒粗化出现软化区域，其显微硬度值略低于基体.

(4) 在战场或野外环境条件下，作为一种应急焊接维修工艺，水蒸气等离子弧焊能够基本满足 7A52 铝合金应急焊接使用要求.

参考文献：


[1] Thomas W M, Nicholas E D. Friction stir welding for the transportation industries[J]. Materials and Design, 1997, 18(6): 269－273.

[2] Dawes C J, Thomas W M. Friction stir process welds aluminum alloys [J]. Welding Journal, 1996, 75(3): 41－45.

[3] Joelj D. The friction stir welding advantage[J]. Welding Journal, 2001, 80 (5): 30－34.

[4] 梁桂芳. 切割技术手册[M]. 北京：机械工业出版社，1999.

[5] 崔信昌. 等离子切割与焊接[M]. 北京：国防工业出版社，1980.

[6] 赵 勇，付 娟，张培磊，等. 焊接方法对 6061 铝合金接头性能影响的研究[J]. 江苏科技大学学报(自然科学版)，2006，20(1)：90－94.
Zhao Yong, Fu Juan, Zhang Peilei, *et al*. Study on effect of 6061 aluminum alloy welded joint properties by welding ways[J]. Jiangsu Scientific and Technical University (Natural Science Press), 2006, 20(1): 90－94.

[7] 黄兰萍，陈康华，李 松，等. 高温预析出对 Al-Zn-Mg 铝合金组织、力学性能和应力腐蚀性能的影响[J]. 中国有色金属学报，2005，15(5)：727－733.
Huang Lanping, Chen Kanghua, Li Song, *et al*. Effect of Al-Zn-Mg aluminum alloy microstructure, properties and SCC by high temperature pre-precipitation[J]. Nonferrous Transaction of China, 2005, 15 (5): 727－733.

[8] Chen Kanghua, Huang Lanping. Strengthening toughening of 7×× × series high strength aluminum alloys by heat treatment[J]. Transaction Nonferrous Meterials Science China, 2003, 13(3): 484－494.

[9] 余 进，王克鸿，徐越兰，等. 7A52 铝合金双丝焊接头的组织及性能[J]. 焊接学报，2005，26(10)：87－89.
Yu Jin, Wang Kehong, Xu Yuelan, *et al*. Microstructure and properties of 7A52 aluminum alloy welded joint by twin wire welding[J]. Transaction of the China Welding Institution, 2005, 26(10): 87－89.

[10] 马文姝，白风臣. 金属熔焊原理[M]. 哈尔滨：哈尔滨工程大学出版社，2007.



作者简介：马世宁，男，1941 年出生，本科，教授，博士生导师. 主要从事装备表面工程及装备维修等方面的研究. 发表论文 200 余篇.

Email：mashining@263.net


[上接第 8 页]


[6] Vinogradov A Yu, Stolyarov V V, Hashimoto S, *et al*. Cyclic behavior of ultrafine-grain titanium produced by severe plastic deformation[J]. Materials Science and Engineering, 2001, 318(1－2): 163－173.

[7] Ivasishin O M, Semiatin S L, Markovsky P E, *et al*. Grain growth and texture evolution in Ti-6Al-4V during beta annealing under continuous heating conditions[J]. Materials Science and Engineering, 2002, 337(1－2): 88－96.

[8] 赵 晖，韩 忠，陈晓风. 电子束扫描对 Ti-6Al-4V 合金焊缝组织的影响[J]. 焊接学报，2005，26(1)：78－80.
Zhao Hui, Han Zhong, Chen Xiaofeng. Effect of scanning electron beam on solid field structure of welded Ti-6Al-4V alloy[J]. Transactions of the China Welding Institution, 2005, 26(1): 78－80.

[9] Elmer J W, Palmer T A, Wong Joe. In situ observations of phase transitions in Ti-6Al-4V alloy welds using spatially resolved x-ray diffraction[J]. Journal of Applied Pysics, 2003, 93(4): 1941－1947.

[10] 吴会强，冯吉才，何景山，等. 电子束焊接热输入对 Ti-6Al-4V 组织结构的影响[J]. 焊接学报，2004，25(5)：41－44.
Wu Huiqiang, Feng Jicai, He Jingshan, *et al*. Effects of electron beam heat input mode on microstructure of Ti-6Al-4V[J]. Transactions of the China Welding Institution, 2004, 25(5): 41－44.

[11] Elmer J W, Palmer T A. Phase transformation dynamics during welding of Ti-6Al-4V[J]. Journal of Applied Physics, 2004, 95(12): 8327－8339.

[12] Deng Anhua. Martensitic transformation of titanium alloys[J]. Shanghai Nonferrous Metals, 1999, 20(4): 193－199.



作者简介：吴 巍，男，1976 年出生，博士. 主要从事钛合金焊接冶金过程的研究. 发表论文 6 篇.

Email：wuwsw@163.com

# MAIN TOPICS, ABSTRACTS & KEY WORDS

**Time-sharing controlled frequency multiplication of IGBT based 180 kHz/50 kW high frequency induction soldering power supply**

SHEN Jinfei, HUI Jing, WU Lei, YAN Wenxu (School of Communication and Control engineering, Jiangnan University, Wuxi 214122, Jiangsu, China). p 1—4

**Abstract**: In order to increase the inverter of output frequency of an IGBT based, the IGBT current must be enlarged extremely, however, nowaday, the increase of output frequency is limited. Carrying on two groups of inverters by the time-sharing controlled technology may multiply the output frequency of IGBT based inverter. A novel 180 kHz IGBT based high frequency soldering power supply was presented, which applied by frequency multiplication and time-sharing control. The power supply has two paralleled IGBTs in each inverter bridge arm in charged by the time-sharing control, therefore each IGBT operates at half frequency, and the switch loss reduces half too. The inverter operates at double times of each inverter group and achieves at the frequency of 180 kHz. While the load of soldering power of 50 kW in series-resonance conditions, each IGBT operates under the condition of ZCZVS turn-on and ZVS turn-off. Working principles and the parameters of main circuit and the control frames and the experiment waveforms are given.

**Key words**: frequency multiplied inverter; soldering power supply; IGBT time-sharing control

**Influence of elevated temperature holding time on microstructure and properties in heat affected zone of fine grained titanium alloy**

WU Wei, GAO Hongming, CHENG Guangfu, WU Lin (State Laboratory of Advanced Welding Production Technology, Harbin Institute of Technology, Harbin 150001, China). p 5—8, 12

**Abstract**: The influence of elevated temperature holding time ($t_\beta$) on grain growth, microstructure transformation and mechanical properties in heat affected zone of fine grained Ti-6Al-4V alloy with equiaxed crystal has been investigated using thermal simulation testing machine. Results show that grains in coarse grained region have been coarsened seriously and the intracrystalline $\alpha'$ is composed of orthogonally oriented martensitic plates which have a substructure containing predominately twins with longer $t_\beta$; Grain growth tendency is relatively little and its morphological features of intracrystalline $\alpha'$ present lath martensites which have a substructure containing predominately dislocations with medium and shorter $t_\beta$; Continued increases in $t_\beta$ results in a reduction in the hardness of coarse grained region; Finer grains, intracrystalline $\alpha'$ martensites having dislocation substructure induced by shorter $t_\beta$ result in higher mechanical properties than martensitic plates which have substructure containing twins with higher $t_\beta$ in coarse grained region.

**Key words**: fine grained titanium alloy; coarse grained region; grain growth; martensite; substructure

**Microstructures and properties of 7A52 aluminum alloy welded joint by vapor plasma arc welding**

MA Shining, LUO Lin, QIU Ji, LIU Qian (1. Faculty of the Remanufacturing Engineering, Armored Engineering Institute, Beijing 100072, China). p 9—12

**Abstract**: 7A52 aluminum alloy plate of 10 mm was welded by vapor plasma arc welding with ER5356 filler and 40% acetone $H_2O$ solution. The mechanical properties and microstructure of the welded joint were studied. The results indicate that the welded joint shows sound mechanical properties. Micrograph analysis shows that the tensile fracture exhibits large quantities of dimples, which indicates good ductility of the weld. There is a softening zone in the HAZ. No abnormal porosity, inclusions and micro-cracks were found in the welded joint. Therefore, vapor plasma arc welding of 7A52 aluminum alloy can obtain excellent welded joint.

**Key words**: 7A52 aluminum alloy; vapor plasma arc welding; welded joints; microstructure

**Mechanism of $CsF-AlF_3$ and $KF-AlF_3$ fluxes reacting with oxide films of 6063 aluminum alloy**

ZHU Hong[1,2], XUE Songbai[1], SHENG Zhong[1] (1. College of Materials Science and Technology, Nanjing University of Aeronautics and Astronautics, Nanjing 210016, China; 2. 14th Research Institute, China Electronic Technology Group Corporation, Nanjing 210013, China). p 13—16, 20

**Abstract**: $CsF-AlF_3$ flux and $KF-AmF_3$ fluxes were selected, the effects of removing the oxides on the surface of 6063 aluminum alloy by these two fluxes were studied at different temperatures, and then the reaction mechanism between flux and surface oxide film of 6063 aluminum alloy was analyzed and discussed. It is discoved that the oxide film on the surface of 6063 aluminum alloy was removed by $CsF-AlF_3$ flux in a reacting and/or dissoluting way, and the HF formed at high temperature from $NH_4F$ was the critical compounds existed in the $CsF-AlF_3$ flux. In addition, the formation of HF was improved and accelerated duo to the $H_2O$, hence the process of removing the oxides was accelerated by the flux. The CsF and $AlF_3$ were not found, and only a few amount of $CsAlF_4$ was found in the residuai of $CsF-AlF_3$ flux, and also, the main residua of $KF-AlF_3$ flux was $KAlF_4$ at the 570 ℃, KAlF4 was not found at the 610 ℃, which only a few amount of $KMgF_3$ was found. Results also indicated that in the residua of $KF-AlF_3$ flux, Mg, Mn and $KAlF_4$ would loss gradually, which lead to the melting point of flux increasing rapidly and the flux fluidity became poorer.

**Key words**: 6063 Al alloy; oxide film; flux; residua